Available online at www.sciencedirect.com
SCIENCE DIRECT®
Journal of Sound and Vibration 289 (2006) 278–293
JOURNAL OF SOUND AND VIBRATION
www.elsevier.com/locate/jsvi

Design of an optimal shock-damping isolator with application to casters

Runling Pan, Jin Jiang*, Ralph O. Buchal

Faculty of Engineering, The University of Western Ontario, London, Ontario N6A 5B9, Canada

Received 23 February 2004; received in revised form 28 January 2005; accepted 6 February 2005
Available online 29 March 2005

Abstract

Design of an optimal shock-damping isolator is presented in this paper with specific application to casters. The design is first formulated as an optimization problem to minimize the peak acceleration of a load while keeping the maximal deflection of the isolator within a specified physical limit. The resulting solution is a constant force isolator. However, it is difficult to realize a constant force isolator with conventional mechanisms using linear springs and dampers. To implement such an isolator physically, a novel mechanism employing multiple linear springs has been developed. The structure and the parameters of the springs have been chosen by optimization techniques, and the resulting mechanism has been embodied in a prototype caster design. This paper presents the concept, design procedure, simulation and experimental evaluation results of a prototype optimal shock-damping caster in detail. The peak acceleration of this new design is only 65% of the existing caster. From a manufacturing point of view, this newly designed caster is not much more complex than existing ones.

1. Introduction

Delicate equipment may be very sensitive to shocks and prone to shock-induced damage. In practice, protective devices are often used to minimize potential shocks in such situations. For movable platforms, one of the solutions is to mount shock-absorbing casters on the bottom of the

*Corresponding author. Tel.: +1 519 661 2111x88320; fax: +1 519 850 2436.
E-mail address: jjiang@eng.uwo.ca (J. Jiang).

0022-460X/$ - see front matter © 2005 Elsevier Ltd. All rights reserved.
doi:10.1016/j.jsv.2005.02.006

cart. For example, such casters can be found in hospitals to transport sensitive equipment, or even patients, and on factory floors to move precision machinery and instruments. Even though casters come in different shapes and sizes, most of them reply on spring and damper (often made of rubber) mechanisms to absorb the energy induced from shocks. The shock-absorbing efficiency of this type of caster is determined by the resilient characteristics of the springs and the cushioning rubber in the dampers. To achieve desired performance, the amount of spring deflection is also an important factor to be considered. Generally speaking, increasing spring deflection improves the shock-absorbing capability, but also increases the size of the caster. However, in many circumstances, constraints on physical dimensions may prevent one from using over-sized casters. Hence, it is important to find new ways to improve the shock-damping capability of a caster without significant increase in the spring travel. The performance of such shock isolators can be optimized to a certain extent by using optimal shock isolation mechanisms. The objective of this paper is to investigate the design of such an optimal isolator.

Generally speaking, shock isolators can be classified into three categories, namely passive, active and semi-active [1,2] isolators. Traditional passive isolators consist of springs that are used to temporarily store the shock-induced energy and dampers in which this energy can be gradually dissipated. They offer a simple and reliable means to protect the load from shock-induced damage [3,4]. However, their performance may be limited under severe shock conditions. There has been extensive research into the use of feedback control techniques to improve the shock isolation capabilities by employing actuators, sensors and real-time controllers. These isolators are known as active isolators [5–9]. Active isolators, if designed properly, may provide superior performance to passive isolators, because they rely on separate energy sources (power from the actuators) to compensate for shocks. However, active isolators are usually complex, expensive and may run the risk of instability due to time-delays in the feedback loop, or in the event of sensor and actuator malfunctions. Semi-active isolators provide a compromise between active and passive isolators [10–13]. A typical semi-active isolator consists of a passive spring in parallel with an active damper. The isolator generally requires no external energy source. The force characteristics of the damper can be regulated automatically through adjustment of an orifice depending on the caster travel. The isolator considered in this paper belongs to the class of passive isolators.

In this paper, the design of optimal passive shock-damping isolators is examined first from both theoretical analysis and physical implementation points of view. Subsequently, a prototype caster is designed, constructed and tested. Dynamic simulations of the design and extensive experimentation on the prototype caster have been carried out. It is concluded that the newly designed optimal shock-damping caster can reduce the maximal shock to as little as 65% of the peak acceleration of the original design without increasing the size of the caster. Moreover, the new prototype does not significantly increase in the complexity of the caster assembly.

The paper is organized as follows: The problem of shock-damping isolator is formulated in Section 2 as a constrained min–max optimization problem. The solution to this optimization problem is examined in Section 3, with physical explanations. The conceptual design and physical prototyping of the optimal shock-damping caster are discussed in Section 4, where a caster rolling over a bump of measurable height is used as the specific shock input condition. The design of the prototype caster is also described in detail in this section. The results from simulation studies are analyzed in Section 5. The experimental results of the prototype caster are compared with those from an existing caster in Section 6. Finally, conclusions are drawn in Section 7.

2. Formulation of optimal shock isolation problem

The shock isolation problem can be studied by using a single-degree-of-freedom (sdof) system as shown in Fig. 1. The object being protected is represented by the rigid body that is attached to the rigid movable base through the shock isolator. It is assumed that the base moves along the vertical direction and the body can move relative to the base in the same direction. The governing equation of motion for this system is

$$m\ddot{x}(t) + u(x(t) - y(t), \dot{x}(t) - \dot{y}(t), t) = 0, \tag{1}$$

where m is the mass of the body, $x(t)$ represents the displacement of the body, and $y(t)$ represents the displacement of the base which is subjected to external forces or displacement excitations. The second term in Eq. (1), $u(x(t) - y(t), \dot{x}(t) - \dot{y}(t), t)$, represents the total force acting on the mass in a general form, without assuming linearity.

Two criteria are often used in practice to specify the performance of an isolator. They are the peak acceleration of the body, i.e. $\max|\ddot{x}(t)|$, and the peak deflection of the isolator, i.e. $\max|x(t) - y(t)|$. The peak acceleration is proportional to the maximal isolator force acting on the body. If the peak acceleration is too high, damage to the equipment as part of the body may result. The peak deflection of the isolator must be kept within the allowable travel or the range of motion of the isolator. Mathematically, these two performance criteria can be described by [14]

$$J_1 = \max|x(t) - y(t)|, \quad J_2 = \max|\ddot{x}(t)|, \tag{2}$$

where the performance index J_1 defines the peak displacement of the body relative to the base, which is equivalent to the peak deflection of the isolator, and J_2 represents the absolute peak acceleration of the body.

Clearly, the above two objective functions are related through the dynamic characteristics of the isolator. Depending on a specific application, either J_1 or J_2 can be adopted as the main performance criterion in the isolator design, while the other acts as a constraint. For example, the peak acceleration can be used as the primary design criterion, where a stringent limit on the acceleration is imposed. On the other hand, if the size of a caster is of primary consideration,

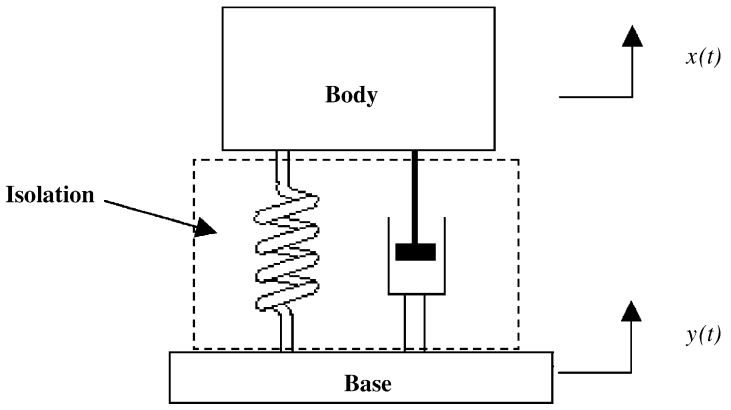

Fig. 1. Single dof model of shock isolator; $x(t)$ is the displacement of the body and $y(t)$ is the displacement of the base.

the peak deflection may be used as the design objective to minimize the travel, hence, the size of the caster.

Since the objective considered in this paper is to minimize the peak acceleration in the event of a shock, the optimization problem is to minimize the performance criterion J_2, while keeping J_1 within an allowable limit for a given level of shock input. This can be formulated as a min–max optimization problem:

$$\text{Minimize}\{\max|\ddot{x}(t)|\}, \text{ under the constraint } \max|x(t)-y(t)| \leqslant D_0, \tag{3}$$

where D_0 denotes the allowable limit on the deflection of the isolator. In this case, the optimization variables are the second term on the left-hand side of Eq. (1), i.e. the internally generated force from the isolator, $u(x(t)-y(t), \dot{x}(t)-\dot{y}(t), t)$.

3. Principle of optimal shock-damping isolators

3.1. Problem description

To achieve effective shock protection, the level and type of external shock excitations should be defined properly in advance. This paper concentrates on a particular type of shock excitation induced when the isolator (caster) rolls over a bump of a certain height traveling at a constant horizontal speed. This mimics many practical situations. This kind of shock excitation has been widely accepted as a standard performance test by caster manufacturers. If the speed of travel is greater than a certain level, the caster will become airborne after hitting the bump, and returns to the surface as a free-falling body. Extensive testing by caster manufacturers has shown that the peak acceleration usually occurs at the moment of impact when the isolator hits the surface again. Therefore, in this paper, the shock isolator design is focused mainly on minimizing the peak acceleration at this instant of impact. Furthermore, if the characteristic of the isolator is underdamped, it has been shown [15] that the peak acceleration occurs within the duration of $T/4$ after the initial impact, where T is the natural period of the system. In other words, the peak acceleration occurs during the initial compression phase of the isolator stroke after the impact.

When a free body falls from a height H, the body will have the maximal downward velocity just before the moment of impact. The velocity of the body then decreases to zero by deflecting the isolator. The work, W, done by the force of the isolator to the body is equal to the change in its kinetic energy. Therefore, the following is true:

$$W = mgH, \tag{4}$$

where g is the acceleration of gravity. Different isolators may have different force–displacement trajectories while absorbing the shock-induced energy during the deflection process. For a given amount of shock energy input, an optimal isolator is the one that achieves the minimal peak acceleration among a group of isolators satisfying the condition

$$\int_0^x u(x(t), \dot{x}(t), t)\,\mathrm{d}x = mgH, \tag{5}$$

while $x(t)$ is within a given deflection limit.

It is important to point out that the integrand in Eq. (5) is another way of representing the internal force generated by the isolator. In Eq. (5), the base position $y(t)$ is explicitly represented by $x(t)$ through the isolator dynamic equation. The integration of the force with respect to the displacement is nothing but the amount of energy temporarily stored or dissipated in the isolator. The optimal shock isolator represents a force–displacement trajectory that satisfies Eq. (5), while having the lowest peak acceleration.

Since the above optimization attempts to minimize the maximal acceleration, the characteristics of the solution to this min–max problem are very straightforward. This can be explained intuitively through graphical representations as shown in Fig. 2, where it shows three isolators that all satisfy Eq. (5), but with different dynamic characteristics. These characteristics as labeled 1, 2 and 3, are shown in the acceleration–deflection plane. The shaded area represents the work that has to be done by the isolators (the right-hand side of Eq. (5)). The area under each curve represents the work done by the respective isolator. For a given bump size, the areas under all three curves are equal. Clearly, the isolator resulting in the lowest peak acceleration is the one with a constant force, which is curve 3 in this figure. Although all three isolators absorb and dissipate the same amount of energy while satisfying the same deflection constraint, the peak accelerations for isolators 1 and 2 are greater than that of the isolator 3. If one thinks that the shaded area represents a 'water-bed', the solution satisfies what so-called 'water-bed' effect, i.e. when the acceleration response curve is pushed further down at one deflection, the acceleration at another deflection has to go up. The minimal peak acceleration occurs only when the water is at a constant level. The characteristics of the isolators beyond the limit of travel are not shown here. High peak accelerations could occur if the isolator hits its limits, which is why it is important to respect the deflection constraints in the optimization process.

Physically, the above means that soon after the isolator with the body hits the surface, the optimal isolator starts to generate a constant force to maintain the acceleration of the body at a constant level until the body stops moving, i.e.

$$u(x(t), \dot{x}(t), t) = F_{\text{const}}, \quad t \in (0, T/4), \tag{6}$$

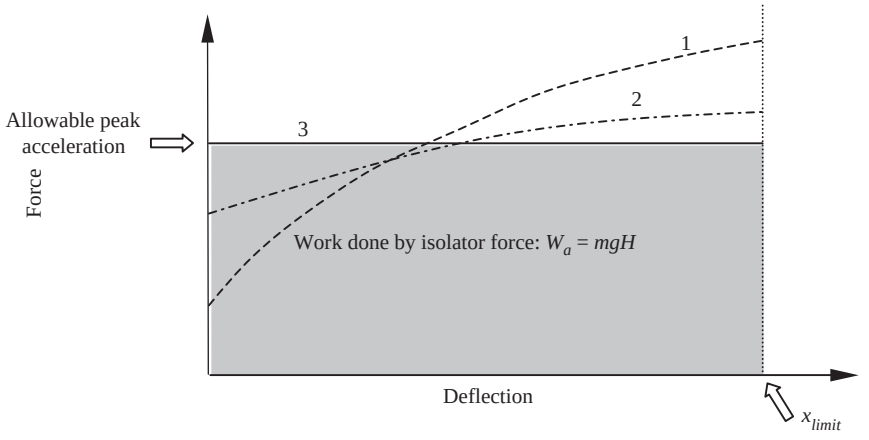

Fig. 2. Three force–deflection curves with equal areas (work done); the curve number 3 has the minimum peak acceleration.

where $u(x(t), \dot{x}(t), t)$ represents the combination of forces from both the spring and the damper in a spring–damper system, and F_{const} is a design parameter to keep the isolator travel $x(t)$ within the given physical limit. For the same deflection and work (area under the force–deflection curve), the peak acceleration for a constant-force isolator can be as low as 50% of the peak acceleration of a linear spring isolator. The question now becomes how to physically realize such a constant force isolator. This will be the subject of the next section.

3.2. Realization of an optimal shock-damping isolator

A constant force isolator cannot be easily realized by using a conventional linear spring and damper mechanism, as the force generated by a spring is proportional to its displacement and the force generated by a viscous damper depends on the velocity of the movement. There are several mechanisms based on spring and linkage structures that can produce a nearly constant force [16]. To implement a nearly constant force, a mechanism using multiple linear springs has been considered in this paper. The overall structure is shown in Fig. 3. The vertically mounted spring is referred to as the main spring and the springs mounted on the sides are called the compensating springs. The parameters L, h and α, are geometric parameters that determine the specific force–displacement characteristics. For easy analysis, the deflection of the main spring is denoted by x_1 and that of the compensating springs by x_2.

The four configurations of the isolator are illustrated in Fig. 3 as the mechanism goes through the compression phase immediately after it strikes the surface. Position (a) represents the first instant of the impact. Once the spring compression begins, the isolator passes through two more stages at positions (b) and (c) until it reaches position (d) at $T/4$. At position (a), the tangent

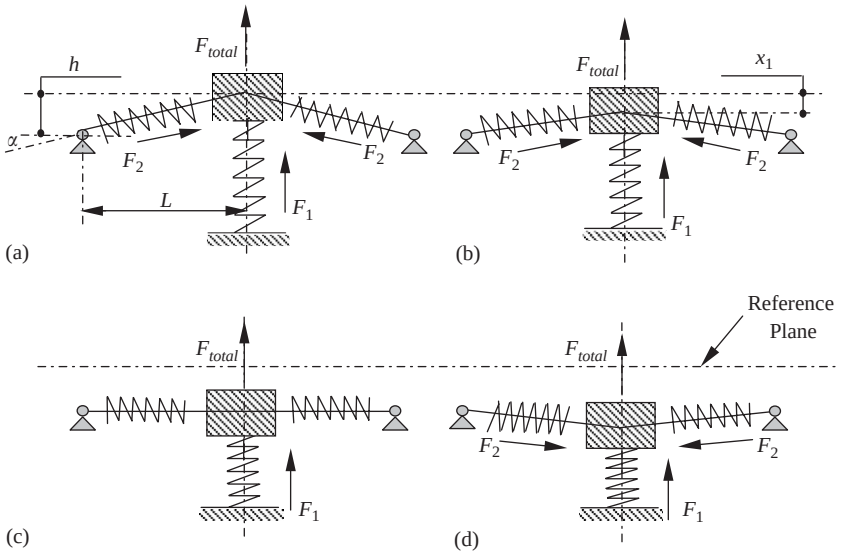

Fig. 3. Multiple-spring system to achieve near-constant force: (a) the first instant of impact; (b) the compression phase; (c) the force toggling position; (d) the phase with reversed force direction.

function of the angle α between a compensating spring and the horizontal reference is

$$\tan \alpha = \frac{h}{L}. \tag{7}$$

At position (b), it can be seen that

$$\tan \alpha = \frac{h - x_1}{L} > 0. \tag{8}$$

At position (c), the compensating springs do not contribute any force component in the vertical direction. It should be noted that this is a unique position, called the toggling position, since from this point onwards, the compensating springs toggle the direction of the vertical force from upward to downward at the position (d):

$$\tan \alpha = \frac{h - x_1}{L} < 0. \tag{9}$$

Because of the toggling behavior of the compensating springs, a nonlinear force–displacement relationship can be achieved using linear compensating springs during the compression process. A nearly constant resultant force can be generated for a finite deflection range by combining the forces from all three springs. Even though no dampers are used in this mechanism, all physical casters have some friction damping. In practice, the magnitude of the damping force is small compared to the spring force; hence, it can be neglected to simplify the analysis.

3.3. Parameter selection for the optimal shock-damping mechanism

As shown previously, the total force generated by the combined springs in the vertical direction depends on several parameters, such as the structural dimensions h and L, spring stiffness k_1, k_2 as well as the spring preload forces F_{preload1}, F_{preload2}. These parameters can be grouped together and represented as the following parameter vector $\mathbf{v}$:

$$\mathbf{v} = [k_1, k_2, h, L, F_{\text{preload1}}, F_{\text{preload2}}]. \tag{10}$$

Consequently, the resultant vertical force generated by the isolator can be expressed as

$$F(\mathbf{v}; x_1), \quad 0 \leqslant x_1 \leqslant x_{1m}, \tag{11}$$

where x_{1m} is the deflection limit of the main spring. If the parameters in $\mathbf{v}$ are chosen properly, a nearly constant force can be achieved in the desired range of the spring deflection. Clearly, the relationships between the desired force and these parameters are nonlinear. Suitable parameters to achieve the desired force–deflection characteristics can be determined by a nonlinear optimization procedure.

For desired deflection–force characteristics (i.e. desired constant force), the parameters can be chosen by using the following least-squares-based optimization:

$$\text{minimize} \sum_{i=1}^{n} [F(\mathbf{v}; x_{1i}) - F_{\text{const}}^{\text{desired}}]^2 \quad \text{for } i = 1, 2, \ldots, n, \tag{12}$$

where the optimization variables are the parameters in the vector $\mathbf{v}$. $F_{\text{const}}^{\text{desired}}$ represents the desired constant force, and n is the number of the data points used in the optimization. The parameters

should also satisfy some physical constraints, e.g. $v_{jL} \leqslant v_j^* \leqslant v_{jU}$ for $j = 1, 2, \ldots, m$, where m is the number of parameters, v_{jL} and v_{jU} are the lower and upper bounds in value for each element, respectively. The spring stiffness values k_1, k_2 are restricted to commercially available values.

4. Design and prototyping of an optimal shock-damping caster

4.1. An existing caster design

A caster is a mechanical assembly consisting of the following elements: a top plate, yoke, wheel, wheel bearing, thread guards, axle nuts and washers. A typical caster is shown in Fig. 4.

The kinematic model of the existing Darcor SL404 caster is shown in Fig. 5. Two springs are mounted in parallel between the pivot O_1 and the moving end B. Assuming that $|OA| = p$, $|OO_1| = q$, $|OC| = l$ and using the moment static equilibrium law, the following can be established:

$$\mathbf{p} \times \mathbf{F}_{s1} = \mathbf{l} \times \mathbf{F}, \tag{13a}$$

where $\mathbf{F}_{s1}$ is the spring force and $\mathbf{F}$ is the total force acting on the body that rests on the caster including the gravity component.

4.2. Converting an existing caster to a constant force caster

Even though one could design a new optimal shock-damping caster based on the principles presented so far, in the current research, it was decided to modify an existing caster to realize the optimal design. There are two reasons for this decision: (1) it allows easy comparison of the performance between the existing caster and the new design, and (2) it reduces the cost of prototyping by using the components already available from the existing caster.

The principle of the optimal isolator presented previously can be readily applied to designing optimal shock-damping casters. The design objective is for the modified caster to produce only half the peak acceleration of the existing caster for the same shock input and peak deflection.

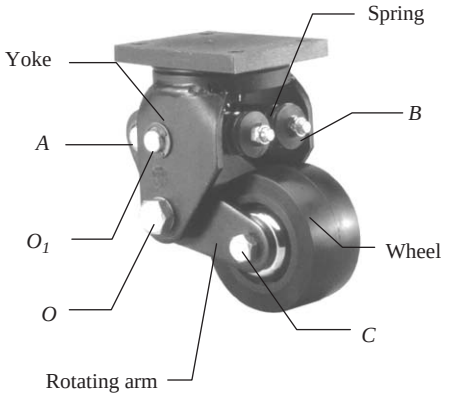

Fig. 4. An existing caster (Darcor SL404).

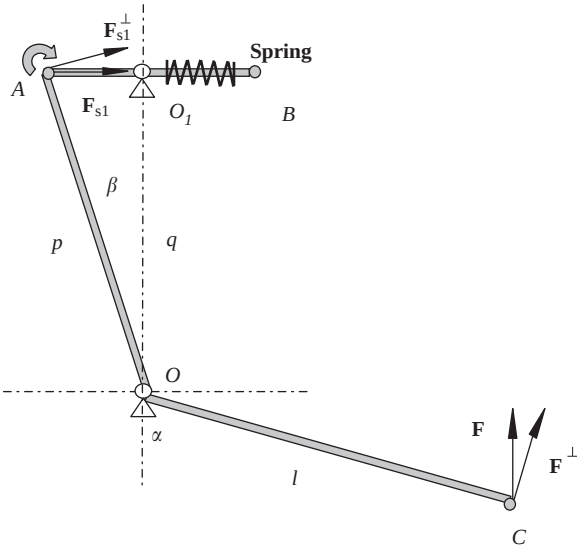

Fig. 5. Kinematic model of the existing Darcor SL404 caster.

Based on this design objective, the required constant force can be determined as follows. For a 100 kg body running over a 1″ bump at a speed 3 km/h, the peak acceleration is 6 g with the original caster. With the optimal caster design, the peak acceleration will be about 3 g. This means that, after taking into account the gravity load, a desired constant force of approximately 4000 N is needed, which has to be generated by the optimal caster.

Although the principle of a multiple spring-based constant force shock isolator is illustrated in Fig. 3, the actual implementation need not resemble this configuration exactly. In fact, a possible mechanism based on modifying an existing caster using multiple springs is illustrated in Fig. 6. O_2 is one end of the compensating spring while D, D' and D'' represent three different positions at the other end. In this case, D is the initial position, D' stands for the toggling position and D'' refers to a point after the toggling. The compensating springs will produce counter-clockwise moments beyond the toggling point. The toggling angle between OD and OD' is defined as θ_t. $\mathbf{F}_{s2}$ represents the compensating spring force and $\mathbf{F}_{s2}^{\perp}$ represents the component of $\mathbf{F}_{s2}$ perpendicular to link OD. The bold arrows represent the directions of the spring moments. The resultant spring force consists of $\mathbf{F}_{s1}$ from the main spring and $\mathbf{F}_{s2}^{\perp}$ from the compensating spring. Note that the deflection limit has now become the limit on the angle θ_t.

Theoretically, D and O_2 can be placed anywhere on two concentric circles centered at O, such that D, O_2 and O are collinear. In practice, they are located to satisfy the physical constraints of the caster design.

4.3. Mathematical model and parameter optimization

The static equilibrium equation of the modified caster can be expressed as

$$\mathbf{p} \times \mathbf{F}_{s1} + \mathbf{r}_1 \times \mathbf{F}_{s2} = \mathbf{l} \times \mathbf{F}. \tag{13b}$$

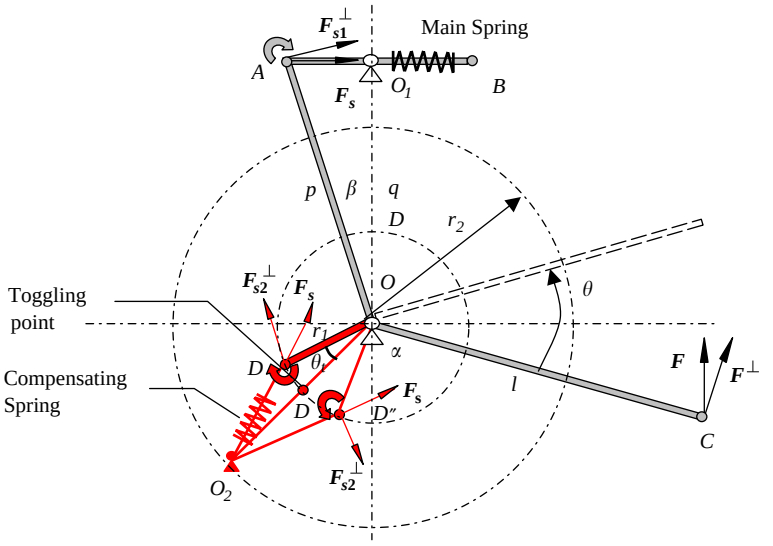

Fig. 6. Kinematic model of modified caster.

No moment is created by the compensating spring at the toggling position since OD' and OO_2 are aligned, hence,

$$\mathbf{r}_1 \times \mathbf{F}_{s2} = 0. \tag{14}$$

After some manipulations, the expression for a nearly constant force F can be expressed as

$$F = \frac{1}{\sin(\theta+\alpha)l}\left\{ p\left(F_{\text{preload1}} + \left[\frac{lF_{\text{const}}^{\text{desired}}\sin(\theta_t+\alpha)}{\cos\left(\frac{\theta_t+\beta}{2}\right)p\Delta x_{1\_t}} - \frac{F_{\text{preload1}}}{\Delta x_{1\_t}} \right]\Delta x_1 \right)\cos\left(\frac{\theta+\beta}{2}\right) \right.$$
$$\left. + r_1(F_{\text{preload2}} + k_2\Delta x_2)\frac{r_2\sin(\theta_t-\theta)}{\sqrt{r_1^2+r_2^2-2r_1r_2\cos(\theta_t-\theta)}} \right\}, \tag{15}$$

where F_{preload1} and F_{preload2} represent the preloads in the main and compensating springs, respectively. Δx_{1_t} is the compression of the main spring at the toggling position. Δx_1 and Δx_2 are the spring deflections, which can be shown to be functions of the geometrical parameters of the system,

$$\Delta x_1 = f_1(p,q,\beta,\theta), \quad \Delta x_2 = f_2(r_1,r_2,\theta_t,\theta). \tag{16}$$

Clearly, the force F is a nonlinear function of the system parameters as shown in Eqs. (15) and (16). It depends on the following parameters: r_1, r_2, θ_t, k_2, F_{preload1}, F_{preload2}, α, β, p, q and l. The independent variable is θ, which represents the angular deflection of the rotating arm from its fully extended position. Let $\mathbf{v}$ be the parameter vector,

$$\mathbf{v} = [r_1, r_2, \theta_t, k_2, F_{\text{preload1}}, F_{\text{preload2}}, \alpha, \beta, p, q, l]. \tag{17}$$

Then the force acting on the body can be expressed as

$$F = f_3(\mathbf{v}; \theta), \quad 0 \leqslant \theta \leqslant \theta_m, \tag{18}$$

where θ_m is the maximal rotation angle of the turning arm. It corresponds to the maximal deflection.

In order to maintain the original structure of the existing caster, some structural parameters remain unchanged. The optimization has been carried out on the remaining parameters to obtain the desired force characteristics. The optimal parameter values are represented by $\mathbf{v}^* = [r_1^*, r_2^*, \theta_t^*, k_2^*, F^*_{\text{preload1}}, F^*_{\text{preload2}}]$ which minimizes $\sum_i [F(\mathbf{v}; \theta_i) - F^{\text{desired}}_{\text{const}}]^2$ for θ_i, $i = 1, 2, \ldots, n$, while satisfying boundary constraints: $v_{jL} \leqslant v_j^* \leqslant v_{jU}$ for $j = 1, 2, \ldots, m$.

Additional engineering factors have to be considered when modifying the existing caster, including available clearance and interference between the moving parts, and commercial availability of springs with the chosen spring stiffnesses. The optimal feasible parameters are shown in Table 1.

Based on the analysis in this section, a modified caster has been designed and constructed as shown in Fig. 7.

5. Simulation results

5.1. Shock damping tests

The simulations of bump tests were conducted using MSC Dynamic Designer [17] motion analysis software. The acceleration and deflection responses for both the existing and the modified

Table 1
Optimal design parameters

r_1^*	r_2^*	θ_t^*	k_1	F^*_{preload1}	k_2^*	F^*_{preload2}
35 mm	70 mm	15°	111 N/mm	750 N	353 N/mm	3000 N

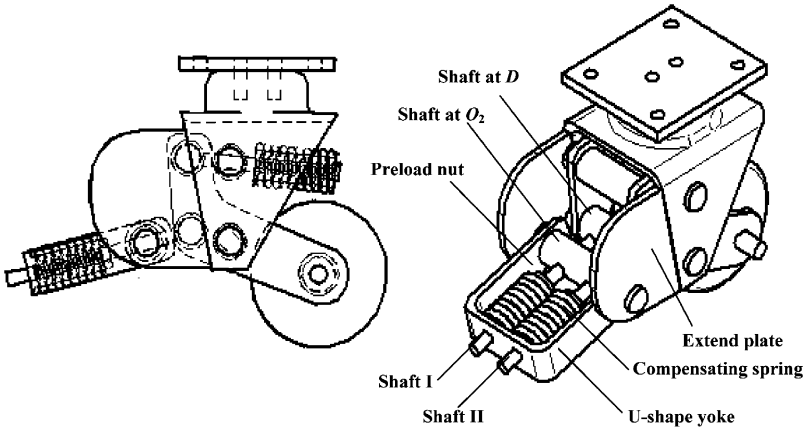

Fig. 7. The modified caster.

casters are shown in Figs. 8 and 9, respectively. In Fig. 8, the first spike of acceleration occurs when the caster hits the bump for the first time. The caster then goes airborne and becomes a free-falling body with gravitational acceleration of $-g$. The second and largest peak acceleration occurs when the caster impacts the surface after the first bounce. The caster bounces several more times, with gradually decreasing acceleration peaks. The maximal peak acceleration of the optimal caster is $3.05g$, which is about 53% of the maximal peak acceleration of the original caster of $5.79g$. Fig. 9 shows a comparison of the deflections. In this figure, the resting (uncompressed) height is 100 mm. Peaks correspond to the caster becoming airborne, and valleys indicate

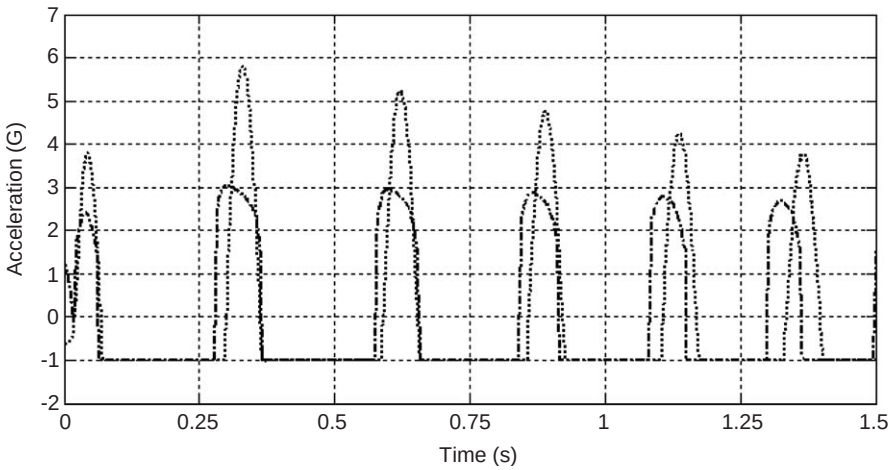

Fig. 8. Simulated acceleration response to a bump test for the original (dotted line) and the modified (dot and dashed) casters.

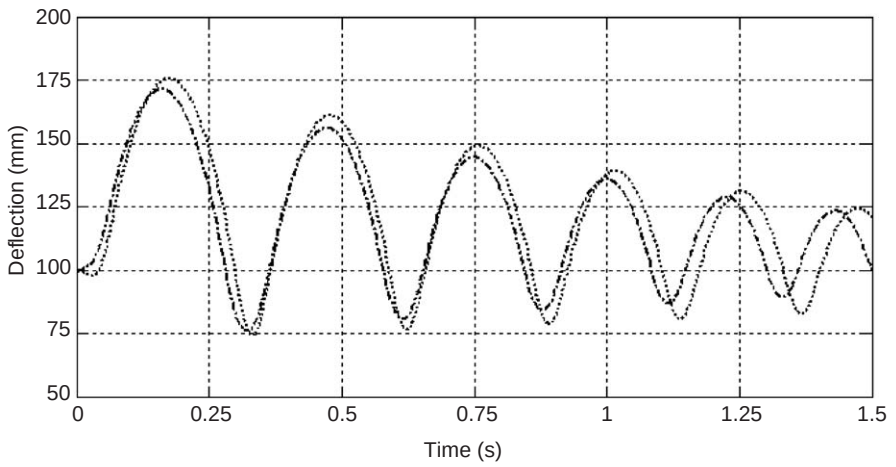

Fig. 9. Simulated deflection response to a bump test for the original (dotted line) and the modified (dot and dashed line) casters.

spring compression or deflection. Both casters have the similar maximal peak deflections of approximately 24 mm.

6. Experimental results

As a part of this investigation, a comparison of experimental and simulated load–deflection curves for the existing caster is shown in Fig. 10 and the modified caster is shown in Fig. 11.

The modified caster exhibits a softening spring characteristic, but it is not quite an ideal constant-force spring. There is reasonable agreement between the simulation and experimental results, with some deviation due to approximations made in the modeling process. The areas under the curves for the existing and modified casters are about the same for a deflection of 22 mm, thus absorbing about the same amount of energy. However, the peak load of the modified caster is 5100 N, which is about 65% of the 7900 N peak load of the existing caster.

The experimental acceleration responses for both the existing and the modified casters under identical shock conditions (i.e. 100 kg load, 1″ bump and 3 km/h speed) are compared. Typical results for seven consecutive bump tests are illustrated in Fig. 12. For each experiment, data are collected from seven impacts to determine the average peak acceleration, and the standard deviation.

Since the experimental evaluations were conducted in the testing center of a caster manufacturer, we were limited by the existing equipment available to us at the time. The sampling frequency used for data collection was 50 Hz, which is too low to accurately locate the exact peaks of the signal. A correction factor of 7% has been added to compensate for this effect.

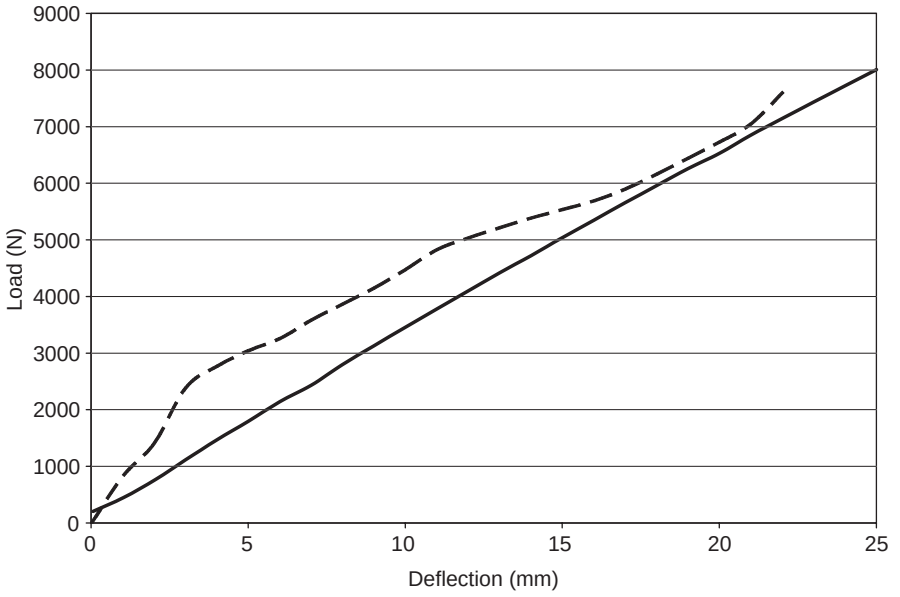

Fig. 10. Simulated (solid line) and experimental (dashed line) load–deflection curves for the existing caster.

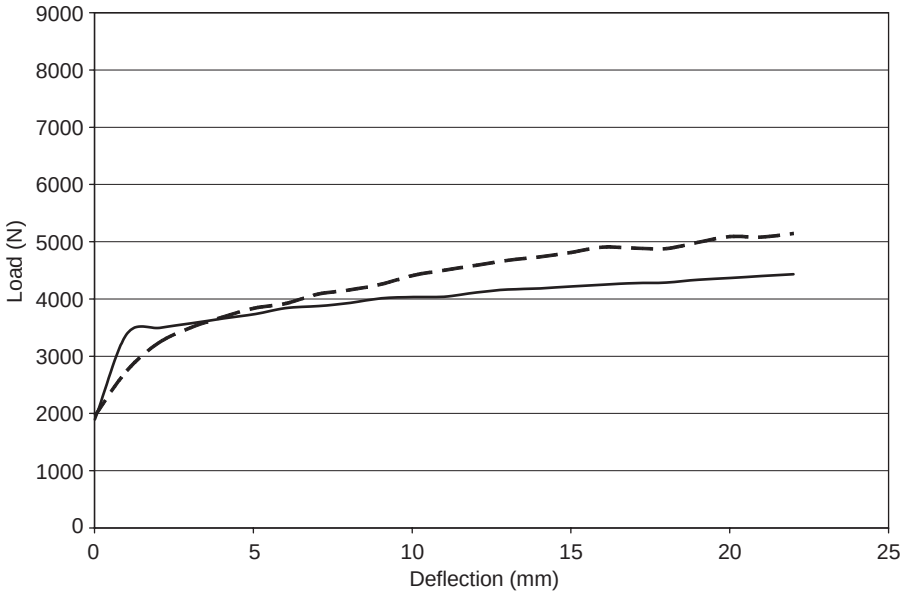

Fig. 11. Simulated (solid line) and experimental (dashed line) load–deflection curves for the modified caster.

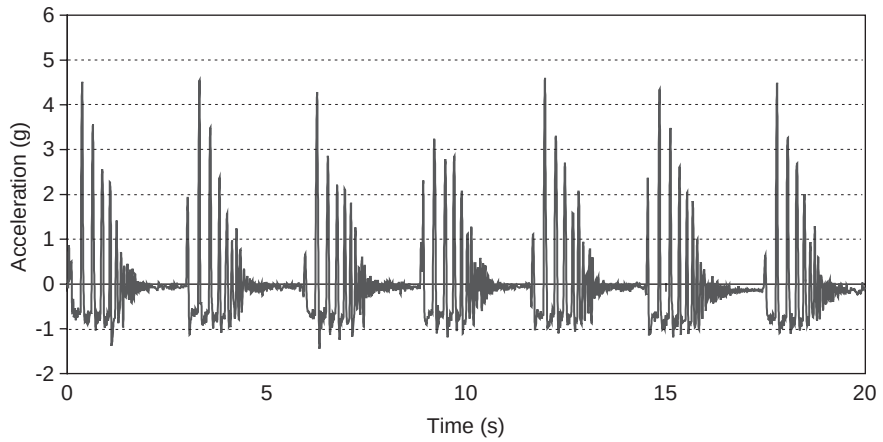

Fig. 12. Typical experimental acceleration response.

The simulated and experimental peak accelerations for the existing and modified casters are compared in Fig. 13. The simulated peak accelerations are higher than the experimental average peak accelerations, but are well within three standard deviations of the measured data. The corrected experimental results show the peak acceleration of the modified caster to be 2.94g, which is only 63% of the peak acceleration of the existing caster.

Even though it has been shown, both by simulation and physical construction/evaluation that the proposed caster design can reduce the peak shock effectively, there are two potential

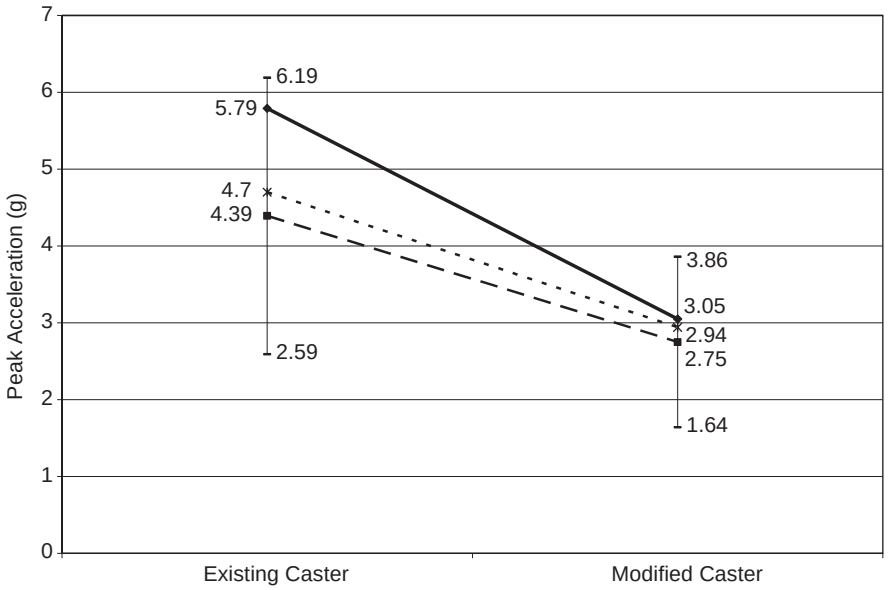

Fig. 13. Simulated (solid line), experimental (dashed line) and corrected experimental (dotted line) peak acceleration for existing and modified caster. Three-sigma error bars are shown for experimental results.

drawbacks that should also be mentioned. The first one is that, if the actual shock disturbance happens to be considerably higher than what has been assumed in the design, the proposed caster could result in a higher shock when the deflection limit is reached. The other corresponds to the situation that if the actual shock disturbance is less than what was assumed in the design, this caster may result in a higher (designed) acceleration than that of a conventional caster. In other words, the proposed design procedure leads to optimal performance when the operating environment of the caster is close to that of the design condition.

7. Conclusions

In this paper, the principle of optimal shock-damping isolators is examined as an optimization problem. A novel design for such an optimal shock-damping caster is presented based on the principle of constant-force isolators. A near constant-force design is achieved using a multiple spring mechanism with a toggling action. A prototype caster has been constructed by modifying an existing caster. The parameters are determined by a least-squares-based optimization. The performance of the modified caster is evaluated against the existing caster under exactly the same conditions in simulations and experimentally. The experimentally determined peak acceleration of the modified caster is only 63% of the peak acceleration of the existing caster. An experimental load–deflection test shows that the modified caster is not quite a constant-force damper; however, the peak force is also reduced to about 65% of the peak force of the existing caster at the same deflection. The experimental data shows that the performance of the prototype is slightly inferior

to what was obtained in the simulation due to unmodeled friction and other nonlinearities in the physical construction. Nonetheless, significant improvement in performance has been achieved with relatively modest and inexpensive design modifications to the existing caster.

Acknowledgements

This work was part of a Materials and Manufacturing Ontario (MMO) Collaborative Research project with Darcor Casters Inc. We wish to acknowledge the assistance and contributions of Mr. Adrian Steenson and Mr. Sayed Azizi of Darcor.

References

[1] L.R. Miller, Tuning passive, semi-active and fully active suspension systems, *Proceedings of the 27th Conference on Decision and Control*, Austin, Texas, 1988, pp. 2047–2053.
[2] R.A. Williams, Electronically controlled automotive suspensions, *Computer and Control Engineering Journal* 6 (1994) 143–148.
[3] C.M. Harris, *Shock and Vibration Handbook*, McGraw Hill, New York, 1996.
[4] D.J. Inman, *Engineering Vibration*, Prentice-Hall, Englewood Cliffs, NJ, 2001.
[5] D.C. Karnopp, Active and passive isolation of random vibration, *Vehicle System Dynamics* 16 (1973) 355–380.
[6] G. Thompson, An active suspension with optimal linear state feedback, *Vehicle System Dynamics* 5 (1976) 187–203.
[7] D.C. Karnopp, Active damping in road vehicle suspension systems, *Vehicle System Dynamics* 12 (1983) 219–316.
[8] E.M. Elbeheiry, D.C. Karnopp, Optimal control of vehicle random vibration with constrained suspension deflection, *Journal of Sound and Vibration* 189 (1996) 547–564.
[9] D. Hrovat, Survey of advanced suspension development and related optimal control applications, *Automatica* 33 (1997) 1781–1817.
[10] J. Alanoly, S. Sankar, Semi-active force generators for shock isolation, *Journal of Sound and Vibration* 126 (1988) 145–156.
[11] M.J. Crosby, D.C. Karnopp, The active damper—a new concept for shock and vibration control, *The Shock and Vibration Bulletin* 43 (1973) 119–133.
[12] D. Karnopp, M.J. Crosby, Vibration control using semi-active force generators, *ASME Journal of Engineering for Industry* 98 (1974) 914–918.
[13] N. Kurata, T. Kobori, M. Takahashi, N. Niwa, H. Midorikawa, Actual seismic response controlled building with semi-active damper system, *Earthquake Engineering and Structural Dynamics* 28 (1999) 1427–1447.
[14] D.V. Balandin, N.N. Bolotnik, W.D. Pilkey, *Optimal Protection from Impact, Shock and Vibration*, Gordon and Breach Science Publisher, Toronto, 2001.
[15] E. Suhir, Dynamic response of a one-degree-of-freedom linear system to a shock load during drop test: effect of viscous damping, *IEEE Transactions on Components, Packaging, and Manufacturing* 19 (1996) 435–440.
[16] E.I. Rivin, *Stiffness and Damping in Mechanical Design*, Marcel Decker, New York, 1999.
[17] MSC.Dynamic Designer, MSC Software Corporation, http://www.mscsoftware.com, visited January 24, 2005.